Adsorption (2012) 18:75–86
DOI 10.1007/s10450-012-9383-5

Adsorption and diffusion of Xenon in a granulated nano-NaY zeolite

Amir Charkhi · Mohammad Kazemeini · Seyyed Javad Ahmadi · Sareh Ammari Allahyari

Received: 20 July 2011 / Accepted: 16 April 2012 / Published online: 4 May 2012

Abstract Henry's law constant and crystal diffusivity of xenon in the granulated nano-NaY zeolite were measured by the pulse gas chromatography method. For this purpose the moments of response peaks of xenon were analyzed. The effect of extra column parts of the utilized chromatographic system was also considered by analyzing the moments of the response peak which was obtained by pulse injection of inert gas of helium into the carrier gas of nitrogen. In addition, the measurement of average velocity of the carrier gas regarding the pressure drop in the extra column parts of the system attributed to precise results. By carrying out the experiments at various temperatures in the range of 30–110 °C the heat of adsorption and activation energy of crystal diffusivity were estimated. In order to find the binder effect on the adsorption of and diffusion into granules, the aforementioned parameters were also measured for the binderless granules of macron sized NaY zeolite. Results revealed that although the adsorption of xenon on the binder of bentonite was negligible, the diffusion resistance created by this binder was significant such that the effective crystal diffusivity in the granules with 25 % binder was determined to be 96 percent lower than the granules with no binder.

Keywords Crystal diffusivity · Henry's law constant · Pulse chromatography · Nano sized · NaY zeolite · Xenon

A. Charkhi · M. Kazemeini (✉)
Department of Chemical and Petroleum Engineering, Sharif University of Technology, Tehran, Iran
e-mail: Kazemini@sharif.edu

A. Charkhi · S.J. Ahmadi · S. Ammari Allahyari
Department of Nuclear Fuel Cycle, Nuclear Science and Technology Research Institute, Tehran, Iran

Nomenclature

D_{AB}	Molecular diffusivity (m^2/s)
D_{ax}	The axial dispersion coefficient (m^2/s)
D_p	Diffusion coefficient in pores of granules (m^2/s)
D_μ	The effective diffusivities (m^2/s)
$D_{\mu 0}$	Crystal diffusivity constant (m^2/s)
E_μ	The activation energy of crystal diffusivity (kJ/mol)
K	Dimensionless Henry's law constant based upon the crystal volume
K_0	Adsorption constant
K_m	External mass transfer coefficient (m/s)
L	Length of packed column (m)
Q_0	The heat of adsorption (kJ/mol)
R	Radius of granules (m)
Re	Reynolds number ($\rho V \cdot 2R$)/μ
R_μ	Radius of zeolitic crystal (m)
Sc	Schmidt number ($\mu/\rho D_{AB}$)
Sh	Sherwood number ($K_m 2R/D_{AB}$)
T	Temperature (K)
V	Superficial velocity (m/s) under non-isobaric conditions

Greek Letter

ε_b	The bed porosity
ε_p	Granule porosity
μ	Fluid viscosity (kg/m s)
μ_1	The first normalized moment (s)
μ_2'	The second central moment (s^2)
ρ	Density (kg/m^3)
σ	Standard deviation
τ	Tortuosity factor

1 Introduction

The use of nano-zeolite as an adsorbent in sorption processes makes shorter diffusion path length and consequently, damps the mass transfer resistance. In chromatographic separation methods this matter is important to reduce peaks broadening. However, chromatographic columns filled with such nano-sized crystals may suffer some operational problems such as high pressure drops. Thus, in an industrial application, the packing of the column by granulated adsorbate is necessary. Granulation of nano-zeolites may be done by different methods (Kang et al. 2006; Valtchev and Mintova 2001; Tosheva et al. 2000). In some of these methods the mechanical strength was obtained by utilizing inorganic binder such as clay (Charkhi et al. 2010). The knowledge of the various adsorption and diffusion parameters of these granulated adsorbents is necessary to simulate the chromatography separation method which in turn may be performed for process optimization purpose. To achieve this, accurate models and precise corresponding parameters are needed (Schmidt-Traub 2005). These parameters may refer to the film mass transfer, intercrystalline and intracrystalline resistance raised due to diffusion of sorbates through the external film, macropores and micropores of the granulated adsorbent; respectively. Dispersion of the gas stream flowing through a chromatography column also affected the quality of the separation process and should be accounted for. A number of different empirical expressions were previously determined for prediction of the film mass transfer; axial dispersion coefficient and tortuosity factor (Perry and Green 1999; Giddings and Keller 1965; Guiochon et al. 2006). The crystal diffusivity and adsorption parameters may also be predicted by theoretical models such as molecular dynamics simulation (Karger and Ruthven 1992). Nonetheless, these models only provided approximations of real systems. Therefore, the experimental determination of crystal diffusivity and adsorption parameters indeed are necessary for such optimization purposes. For measurement of crystal diffusivity powerful experimental techniques are available. These included such macroscopic methods as membrane permeation, uptake methods as well as chromatographic and microscopic methods such as pulsed field gradient NMR (Karger and Ruthven 1992). The range of diffusivity measured by these techniques is different. Amongst these, the pulse chromatography method widely utilized to determine the Henry's law constant and crystal diffusivity of different adsorbates on the zeolites (Delmas and Ruthven 1995; Denayer and Baro 1997; Inel et al. 2002; Dıaz et al. 2004, 2005; Zhang et al. 2009; Armatas et al. 2005). In this method, after the injection of a small amount of adsorbate into the chromatography column the moments of response peaks were numerically measured and compared with those calculated theoretically. From this comparison a set of adsorption and diffusion parameters were determined. It seemed that this technique was more reliable than the others when the evaluated parameters would be applied in simulation of chromatographic systems. Furthermore, the selected models and assumptions needed might be similar to those applicable for simulation purposes. Ultimately, utilizing the pulse chromatography method, the effective crystal diffusivity and Henry's low constant for xenon in the granulated nano-zeolite were estimated.

2 Methodology

In the moments analyzing method, first an appropriate mass balance formulation considering concentration distribution in the column and particle in the Henry's law limit should be selected. Then the resulting set of governing equations must be solved by the method of Laplace transform (Do 1998). By having the solution in the Laplace domain the theoretical moments might be readily obtained. For an isothermal column filled with granulated zeolite the bi-dispersed solid model with local equilibrium was assumed governing (Do 1998). In this model, macropore diffusion in the void space between the zeolite crystals and micropore diffusion in the channels of the zeolite considered. Therefore, the first normalized (μ_1) and the second central moments (μ_2') of Gaussian response peak were calculated (Do 1998). Also, in selected model it has been assumed that the granules and crystals are spheres of the radii R and R_μ, respectively.

In the real systems, the extracolumn retention and dispersion factors associated with the injector, connections and detectors would cause tailing of the response peak (Perry and Green 1999). Hence, the apparent moments (μ^{app}) defined as follows:

$$\begin{aligned}\mu_1^{\text{app}} &= \mu_1^{\text{col}} + \mu_1^{\text{conc}} + \mu_1^{\text{inj}} + \mu_1^{\text{det}} + \mu_1^{\text{pipe}} \\ &= \mu_1^{\text{col}} + \mu_1^{\text{ext}}\end{aligned} \tag{1}$$

$$\begin{aligned}\mu_2'^{\text{app}} &= \mu_2'^{\text{col}} + \mu_2'^{\text{conc}} + \mu_2'^{\text{inj}} + \mu_2'^{\text{det}} + \mu_2'^{\text{pipe}} \\ &= \mu_2'^{\text{col}} + \mu_2'^{\text{ext}}\end{aligned} \tag{2}$$

where the μ^{col}, μ^{conc}, μ^{inj}, μ^{det} and μ^{pipe} were the moments related to the column, connections, injector, detector and pipes; respectively. These terms except μ^{col} might be summarized as external moments (μ^{ext}).

In order to eliminate extra column effects and calculate the true moments of the column, pulse injection of an inert gas was performed at different flow rates. With the inert tracer meaning no adsorption (*i.e.*; $K = 0$), the following first normalized moment obtained (Do 1998):

$$\frac{(\mu_1^{\text{app}} - \mu_{1,\text{inert}}^{\text{app}})}{[(1-\varepsilon_p)(1-\varepsilon_b)/\varepsilon_b]} = K\frac{L\varepsilon_b}{V} \tag{3}$$

where the V, L, ε_b, ε_p and K were the average superficial velocity, column length, the bed and granule porosity and dimensionless Henry's law constant based upon the crystal volume, respectively. By plotting the left side of Eq. (3) versus $L\varepsilon_b/V$, the Henry's law constant (K) was obtained from the slope of the corresponding line (Do 1998).

By utilizing the response of the exit concentration versus time, the moments might be calculated as follows:

$$\mu_1^{\text{app}} = \frac{\int_0^\infty t \cdot C_b(z,t)dt}{\int_0^\infty C_b(z,t)dt} = \frac{\sum_{i=1}^n t_i C_i \Delta t}{\sum_{i=1}^n C_i \Delta t} \tag{4}$$

$$\mu_2'^{\text{app}} = \frac{\int_0^\infty (t-\mu_1^{\text{app}})^2 \cdot C_b(z,t)dt}{\int_0^\infty C_b(z,t)dt} = \frac{\sum_{i=1}^n (t_i-\mu_1^{\text{app}})^2 C_i \Delta t}{\sum_{i=1}^n C_i \Delta t} \tag{5}$$

The effective crystal diffusivities (D_μ) may be evaluated from the apparent second central moment ($\mu_2'^{\text{app}}$). The effective crystal diffusivity (D_μ) was considered to be the only unknown parameter in obtained equation for the second central moment. For this purpose the experimental apparent second central moment, the Henry's law constant (*i.e.*; calculated from the first normalized moment) and other parameters which are predicted by empirical expressions are substituted into the equation obtained for the second central moments. In this work the axial dispersion coefficient (D_{ax}), film mass transfer coefficient (K_m), diffusion coefficient in pores of granules (D_p) and tortuosity factor (τ) are predicted through the following equations (Perry and Green 1999):

$$D_{ax} = \gamma_1 D_{\text{AB}} + \gamma_2 \frac{V2R}{\varepsilon_b} \tag{6}$$

$$\gamma_1 = 0.45 + 0.55\varepsilon_b \tag{7}$$

$$\gamma_2 = 0.5\left(1 + 13\frac{\gamma_1 \varepsilon_b}{Re{\cdot}Sc}\right)^{-1} \tag{8}$$

$$K_m = \frac{D_{\text{AB}}}{2R}\left(2 + 1.1Re^{0.6}Sc^{0.33}\right) \tag{9}$$

$$D_p = \frac{D_{\text{AB}}}{\tau} \tag{10}$$

$$\tau = \frac{1}{\varepsilon_b} \tag{11}$$

3 Experimental equipment and procedure

A Buck Scientific gas chromatograph, model 910, system equipped with thermal conductivity detector (TCD) and a suitable computer recording system was utilized. A vacuumed stainless steel tube (*i.e.*, column) was well packed with granulated NaY nano-sized zeolite under continuous mechanical vibration. The temperature of the chromatographic system's oven was carefully calibrated and controlled to within ±1 °C. The granulated NaY nano-zeolite with 25 % binder of bentonite was synthesized with the procedure described in the previous work of these authors (Charkhi et al. 2010). The size distribution of granules as well as; crystals were approximated from SEM images through utilizing image processing ability of the MATLAB software as shown in Fig. 1. The granules and bed voidage were estimated from density of zeolite, bentonite and packing of the column. The column density calculated from the column volume and packing weight. Ultimately, the density of zeolite and clay were found from the literature (Breck 1974). Prior to the experimental runs, the chromatography column conditioning was performed at 473 K for 24 hr while helium gas flowed through the column. The experiments were carried out with trace injection of adsorbate or inert gas in the carrier gas of helium or nitrogen by using a ten port valve equipped with a sample loop of 100 µl. The pulse injection of xenon into the carrier gas of helium and pulse injection of

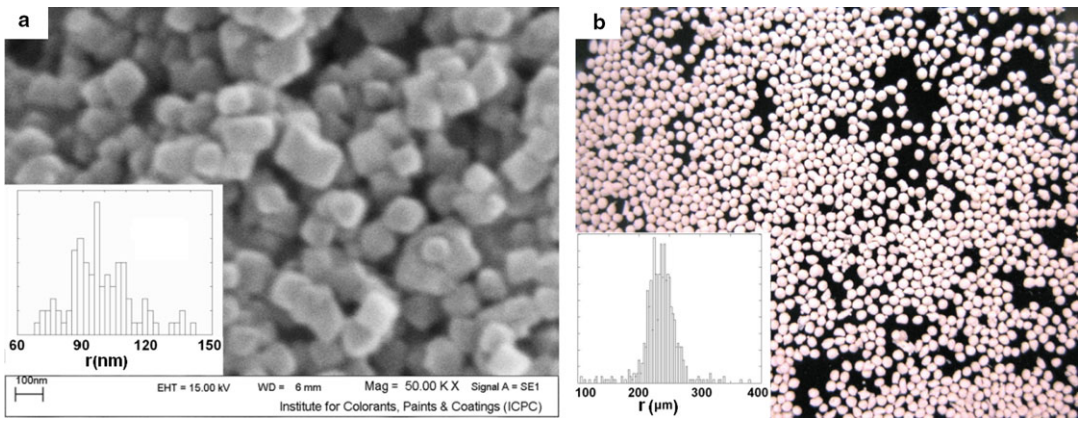

Fig. 1 (**a**) The SEM image of nano-NaY and its size distribution, (**b**) the photograph of granulated nano-zeolite and its size distribution

inert gas of helium into the carrier gas of nitrogen were carried out at different upstream pressures of carrier gas in the range of 12–28 psig and different temperatures in the range of 30–110 °C. The flow rate was measured by a soap bubble meter which placed at the exit pipe of the detector. Since the pressure indicator was placed before the injector, in order to estimate the pressure exactly at the beginning and end of the chromatographic column, the pressure drop at different locations of the system was measured. For this purpose, the flow rate of the carrier gas of helium was measured at different upstream pressures under different states shown in Fig. 2. In the first state the helium flow through the system consisted of a loop, valve, packed column, detector and flow meter while for the second and third states the packed column and loop were removed from the respective cycles. Each set of measurement was repeated four times. In order to estimate the effect of binder on the Henry's law constant and crystal diffusivity, a set of experiments was also conducted by utilizing chromatographic column filled with the binderless granules. For this purpose commercial NaY micron sized zeolite purchased from the Zeolyst company, USA was used instead of nano ones. The reason for replacement of macron sized crystal with nano ones in the binderless granules was due to safety considerations. In other words, the binderless granules due to poor mechanical strength might have gone through aberration and attrition hence producing fine initial powders which if were nanosized could have damaged the TCD rather severely. Furthermore, the Si/Al molar ratio of the commercial zeolite was different from the nano-zeolite. This ratio for the macron and nano-sized NaY zeolite was 2.7 and 1.99; respectively which indicated attention should be paid to this parameter. The injection of xenon into the column filled with binderless granules was performed by 100 µl gas tight Hamilton syringe. Specifications of columns studied also provided in Table 1. The dead volumes of connections and injector before and after the column were determined by measuring the retention times of xenon when the column was removed. Nonetheless, these parts had small volumes, thus, attempts to estimate the dead volume by the aforementioned procedure failed due to the out coming peak being too fast to be resolved. Consequently, the dead volume compared with packed volume (6.13 cm^3) was taken to be negligible.

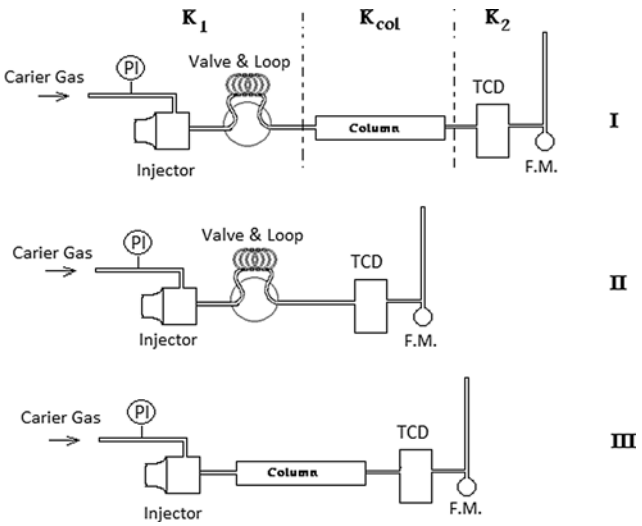

Fig. 2 The various states in the connection of different parts of the chromatographic system investigated in this research

4 Results and discussion

A sample of gas chromatograph recorded by a computer was shown in Fig. 3. In order to eliminate the reverse effect of the base line noise on the calculation of the second central moments; a smooth line was passed through the recorded baseline data and then according to Eqs. (4) and (5) the first normalized and seconded central moments were calculated.

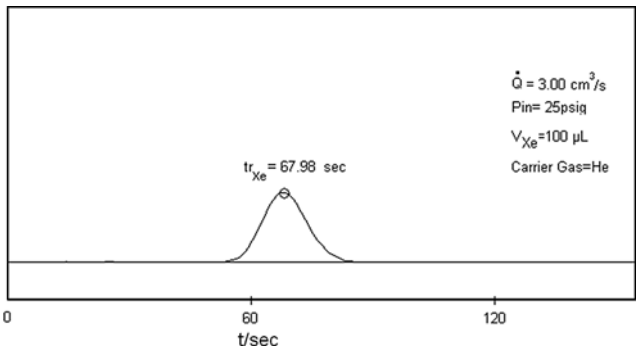

Fig. 3 A sample response peak of the xenon obtained in this research

Table 1 The specifications of column studied in the present study

Packing material	Length (m)	Inner diameter (mm)	Average granule radius[a] (µm)	Average zeolite size[a] (nm)	Granule voidage[b]	Bed voidage[b]	Tortuosity factor
Granulated nano-sized NaY (25 wt% binder)	1.77	2.1	218	98.6	0.47	0.47	2.13
Binderless granulated micron sized NaY	1.77	2.1	80.5	458	0.60	0.41	1.67

[a]Estimated from SEM images

[b]Estimated from density of zeolite (1920 kg/m^3), bentonite (1433 kg/m^3) and column (477.8 kg/m^3)

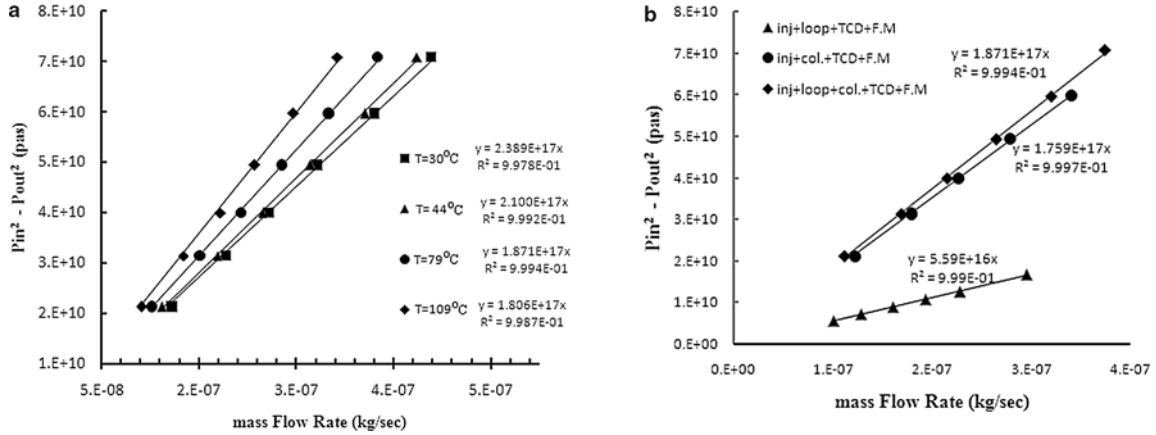

Fig. 4 (**a**) The relationship between the inlet and outlet pressure of the chromatographic system and mass flow rate in the column filled with granulated nano-zeolite and (**b**) under the different states of Fig. 2

Figure 3 showed a sample response peak of xenon for which the flow rate of helium carrier gas was 3 cm^3/s at 30 °C.

Parameters considered here for estimation from the response peaks were the Henry's law constant as well as; the effective diffusivity coefficient. In addition to the terms predicted by Eqs. (6) to (11) and particle and column porosity, the velocity might have also affected the accuracy of the obtained results. Thus, in the column affected by the non isobaric condition, correct determination of average velocity was indeed important. Hence, velocity was calculated with respect to the average pressure determined as follows (Giddings and Keller 1965):

$$P_{\text{avg}} = \frac{2}{3} P_{\text{out}} \frac{(\frac{P_{\text{inc}}}{P_{\text{outc}}})^3 - 1}{(\frac{P_{\text{inc}}}{P_{\text{outc}}})^2 - 1} \tag{12}$$

In the chromatography system utilized in this study as shown in Fig. 2, the inlet pressure was measured before the ten port valve and the atmospheric pressure was the pressure at the exit of the flow meter. Therefore, the inlet and outlet pressures of the column (*i.e.*, P_{inc}, P_{outc}) were calculated through establishing a linear relationship between the mass flow rate and difference of square of pressure of inlet and outlet of the system. This assumption employed in Eq. (13) was plausible for columns with laminar flow. As shown in Fig. 4 by changing the mass flow rate in the range of 1e–7 to 3e–7 kg/s this linear relationship precisely upheld. The mass flow rates obtained through changing the upstream pressure in the range of 10–28 psig. Therefore, simply by measuring the flow rate at the various inlet pressures and different states of Fig. 2 the k constants of the Eq. (13) which are necessary to predict the inlet and outlet pressures of the column were predicted. In this equation $\sum k$ is the summation of k_1, k_2 and k_{col} at the state I, the summation of k_1 and k_2 at the state II and the summation of k_{col} and k_2 at the state III of the Fig. 2. By comparison of $\sum k$ measured at states I and II, and I and III of the Fig. 2; values of k_{col} and k_1 were determined; respectively. According to the calculated k, the inlet and outlet pressure of the column were determined using Eqs. (14) and (15):

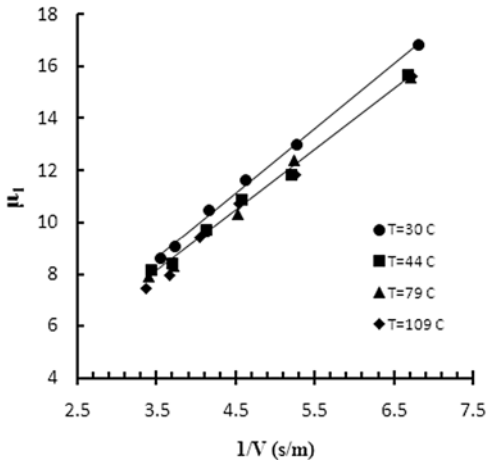

Fig. 5 The first normalized moments of response peaks of helium at various temperatures and velocities

$$P_{in}^2 - P_{atm}^2 = \sum_i k_i \dot{m} \tag{13}$$

$$P_{inc} = \sqrt{P_{in}^2 - k_1 \dot{m}} \tag{14}$$

$$P_{out} = \sqrt{P_{atm}^2 + k_2 \dot{m}} \tag{15}$$

In order to eliminate the effect of extra column parts of a chromatographic system from the moments of response peaks of xenon, the moments of response peaks of helium obtained by the injection of 100 μl helium into the carrier gas of nitrogen were also calculated. The first normalized moments of these peaks at different temperature ranging between 30 to 110 °C were plotted versus the reciprocal ve-

Table 2 Henry's constant for adsorption of Xe in granulated zeolite

T (°C)	Granulated nano-sized NaY (25 % binder)		T (°C)	Binderless granulated micron sized NaY	
	K*	R^2		K*	R^2
30	44.20 ± 0.39	0.9989	30	58.30 ± 0.92	0.9904
44	31.01 ± 0.98	0.9923	38	48.45 ± 0.93	0.9889
79	16.59 ± 0.98	0.8786	44	42.39 ± 0.64	0.9913
109	10.21 ± 0.32	0.9863	50	38.28 ± 0.70	0.9876
			56	32.80 ± 0.66	0.9853
			62	30.34 ± 0.71	0.9807
			79	21.17 ± 0.47	0.9806
			109	14.26 ± 0.57	0.9537

These coefficients obtained with confidence interval of 95 %

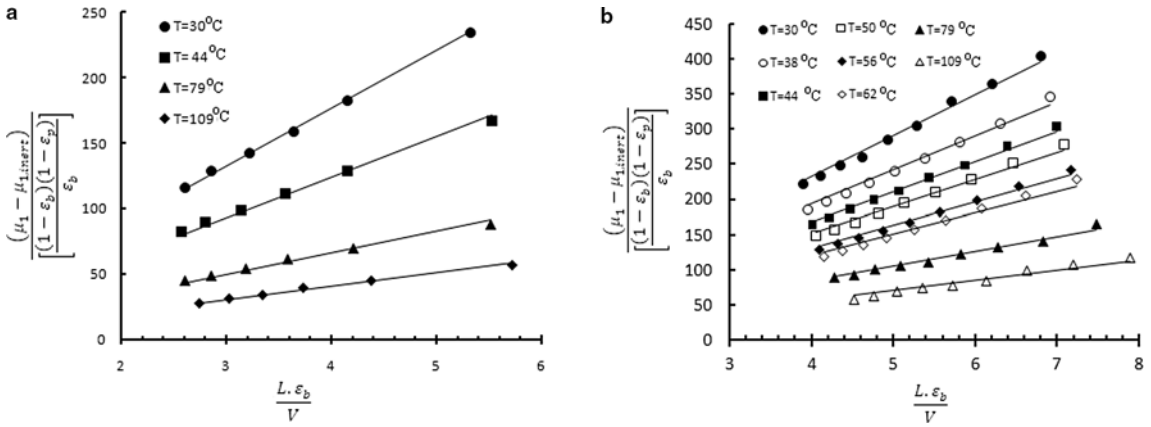

Fig. 6 The left versus right side of Eq. (3) at different temperatures (**a**) the adsorbate of Xe in the granulated nano-NaY zeolite and (**b**) the adsorbate of Xe in the binderless granules of macron sized zeolite

locity shown in Fig. 5. As shown in this figure at a temperature higher than 30 °C the slope of the corresponding lines were constant which indicated that the Henry's law constant of helium over granulated nano-zeolite was negligible and consequently their first normalized moments were only related to the extracolumn effect. Similar results were also obtained for binderless granules of micron sized NaY zeolite. Therefore, by plotting the left versus right side of Eq. (3) at different temperatures as shown in Fig. 6, Henry's law constant was calculated. From the slope of the related line the Henry's law constant for adsorption of xenon over granulated nano-NaY zeolite and binderless granules of micron sized NaY were predicted and results and their corresponding standard deviations provided in the Table 2. Obtained results of the granulated nano-NaY zeolite were more precise than the binderless granules of micron sized NaY. The reason for this latter behavior might have been the various injection methods utilized in each case.

By comparison of the Henry's law constants (K) of granulated nano-NaY and binderless granules of macron sized zeolite, obviously it was observed that the presence of the binder in the nano granules caused lowering of the value of the Henry's law constant. This decrease in K value was nearly equal to what would have been calculated if one assumed the Henry's law constant of bentonite was zero. In this case the K value of granulated nano-NaY zeolite with 25 wt% bentonite had to be 25 % lower than the corresponding value for binderless granules of macron sized zeolite. The obtained results were consistent with this rational. Such a linear relationship between the weight amount of binder and adsorption characteristic of granules was also observed in the adsorption of N_2 at 77 K (Charkhi et al. 2010). In other words; the binder behaved as a true inert diluent with no significant effect on the adsorption properties of nano crystals. The similar behavior also reported for micron sized zeolite in previous work (Breck 1974).

The temperature dependency of Henry's law constant expressed as follows was utilized to calculate the heat of adsorption of xenon over the zeolitic granules.

$$K = K_0 \exp\left(\frac{Q_0}{RT}\right) \tag{16}$$

In this equation; Q_0 is the heat of adsorption and K_0 is the adsorption constant. For estimation of K_0 and Q_0, the logarithm of the Henry's law constant at different temperatures

(Table 2) was plotted versus the reciprocal absolute temperature as shown in Fig. 7. In this figure the minimum and maximum deviations from the mean value were also presented which were indicative of the precision of results obtained in this work. From the slope and intercept of the obtained straight line, the heat of adsorption and adsorption constant determined; respectively. The obtained results were illustrated in Table 3. As shown the heat of adsorption of xenon over granulated nano-NaY zeolite is nearly equal to the heat of adsorption of this component over the binderless granules

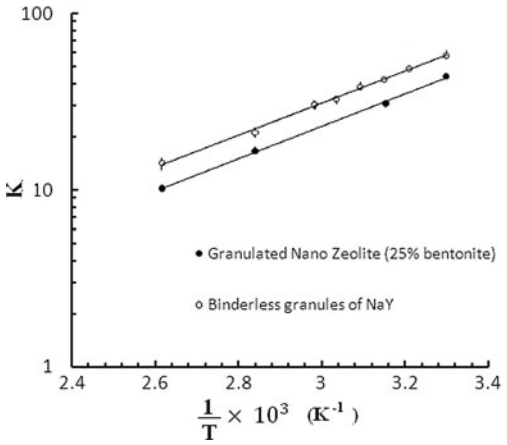

Fig. 7 The effect of temperature on Henry's law constant (K) in granulated nano-NaY (•) and binderless granules of micron sized NaY (○)

of macron sized NaY. According to the values of the Henry's law constant of these two kinds of granules previously discussed, it may again be inferred that the adsorption of xenon on the binder of bentonite was negligible. Also by comparing the heat of adsorptions of the xenon over the NaY and NaX with the Si/Al molar ratio of 1.18 (Breck 1974) it was concluded that in zeolites with the same structural framework, the increase in Si/Al molar ratio led to a decrease of the heat of adsorption. Due to this results, the somewhat of a lower heat of adsorption of macron sized NaY than that of the nano ones might have been attributed to their difference of the Si/Al molar ratio.

The effective diffusivity of xenon in the NaY crystals was evaluated according to the experimental and theoretical second central moments. For this purpose, the Henry's law constant given in Table 2, the experimental second central moments calculated through the Eq. (5) (shown in Fig. 8) and D_p, K_m and D_{ax} predicted by the Eqs. (6)–(11) were substituted in theoretical equation obtained for second central moments and subsequently, R_μ^2/D_μ was calculated at different temperatures and flow rates. Since the zeolitic crystal diffusivity in the Henry's law limit is independent of adsorbate concentration (Do 1998), in this research at each temperature, the value of R_μ^2/D_μ was equal to its average at different flow rates. Furthermore, by replacing the average radius of zeolite crystals instead of R_μ the average effective crystal diffusivity was calculated. The average radius of

Table 3 The heat of adsorption of xenon over the granulated nano-NaY and binderless micron NaY zeolites

Granulated nano-sized NaY (25 % binder)			Binderless granulated micron sized NaY			
$K_0^1 \times 10^2$	Q_0 (kJ/mol)[a]	R^2	$K_0^1 \times 10^2$	Q_0 (kJ/mol)[a]	R^2	Q_0 (kJ/mol)[b]
4.00	17.61 ± 0.38	0.9976	5.75	17.43 ± 0.38	0.9974	20.46

[a]These coefficients obtained with confidence interval of 95 %

[b]These data were obtained for NaX zeolite with the Si/Al molar ratio of 1.18 (Breck 1974)

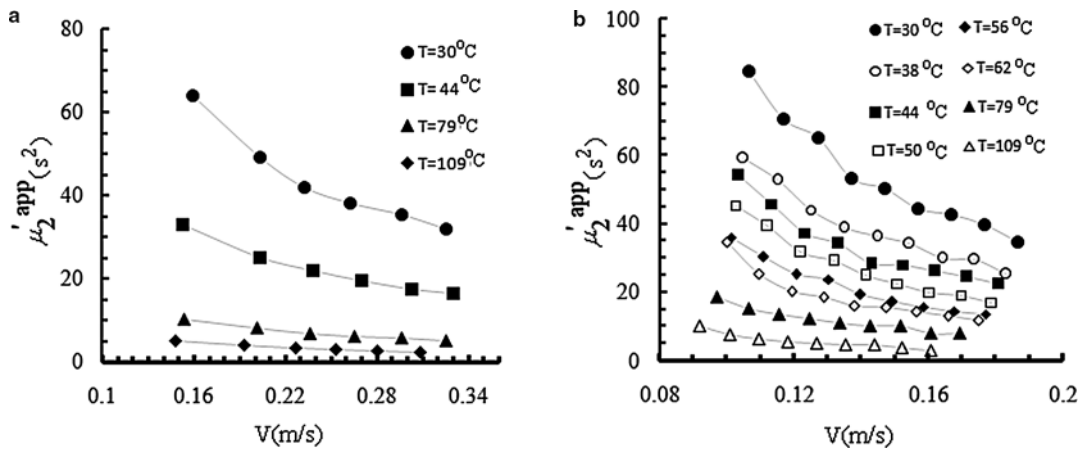

Fig. 8 The experimental apparent second central moments versus superficial velocity

Table 4 The effective crystal diffusivity of xenon into the NaY crystals inserted in the granules

T (°C)	Granulated nano-sized NaY (25 % binder)			T (°C)	Binderless granulated micron sized NaY		
	R^2/D_μ	$D_\mu \times 10^{15}$ (m^2/s)	$\sigma \times 10^{15}$		R^2/D_μ	$D_\mu \times 10^{14}$ (m^2/s)	$\sigma \times 10^{14}$
30	2.74	1.36	0.10	30	2.09	3.87	0.41
44	1.89	1.98	0.15	38	1.85	4.38	0.25
79	1.23	3.03	0.08	44	1.71	4.75	0.36
109	0.94	4.00	0.23	50	1.56	5.18	0.51
				56	1.41	5.72	0.55
				62	1.31	6.15	0.48
				79	1.09	7.39	0.39
				109	0.73	11.04	0.58

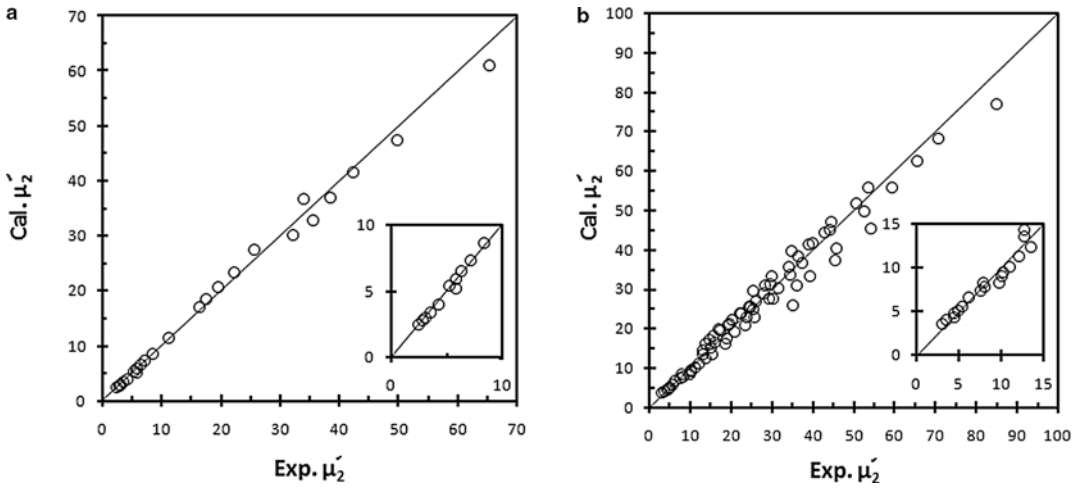

Fig. 9 The calculated second central moments of Xe response peaks versus the experimental results (**a**) Xe over granulated nano-zeolite and (**b**) Xe over the binderless granulated macron sized NaY

zeolitic crystals was obtained by considering that the hypothetical spherical crystals of NaY have the same volume of the real cubic crystals which their average size was given in Table 1. As a result, the average radius of macron sized and nano-sized crystals of NaY measured equal to 61.1 and 284 nm, respectively. The Results and their corresponding standard deviations were indicated in Table 4. It is reiterated that, due to no data found in the literature on diffusivity of xenon in NaY zeolite which was obtained by chromatography method, it was difficult to verify the obtained results in this work. Nevertheless, the order of magnitude of diffusivity obtained in this study nearly agreed with reported data estimated by chromatographic method for other adsorbent or adsorbate (Breck 1974). For example, from the diffusivity of xenon in KA zeolite measured at temperatures above 300 °C it may be predicted that this parameter for this element in KA zeolite at 30 °C would be 6×10^{-14} m^2/s (Breck 1974).

Through comparison of results obtained for granulated nano and macron sized zeolites, it is observed that the presence of the binder in the granules has caused 95.8 % reduction in the effective crystal diffusivity. Thus, it might

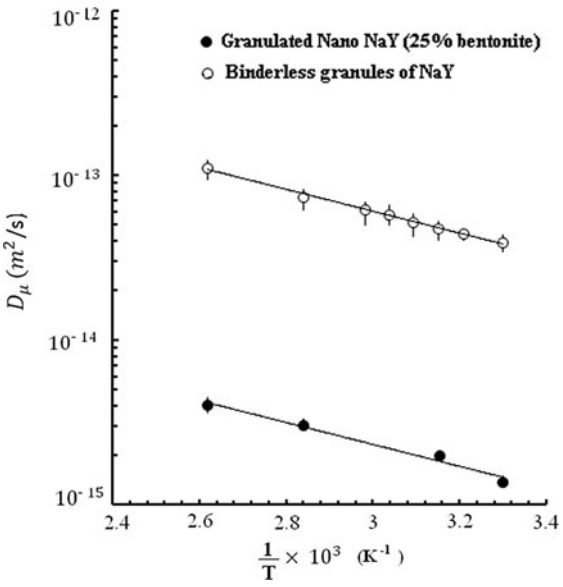

Fig. 10 The temperature dependency of the effective diffusivity of Xe over the nano-NaY zeolite with 25 wt% bentonite (●) and Xe over macron sized NaY zeolite (○)

Table 5 The activation energy of diffusion of xenon into the NaY crystal

Granulated nano-sized NaY (25 % binder)			Binderless granulated micron sized NaY			
$D_{\mu 0} \times 10^{13}$ (m^2/s)	E_μ (kJ/mol)[a]	R^2	$D_{\mu 0} \times 10^{13}$ (m^2/s)	E_μ (kJ/mol)[a]	R^2	E_μ (kJ/mol)[b]
2.32	12.76 ± 0.91	0.9746	57.03	12.63 ± 1.11	0.9977	7.81 ± 0.4[1]

[a]These coefficients obtained with the confidence interval of 95 %

[b]The results obtained from molecular dynamic simulation (Mosell et al. 1996)

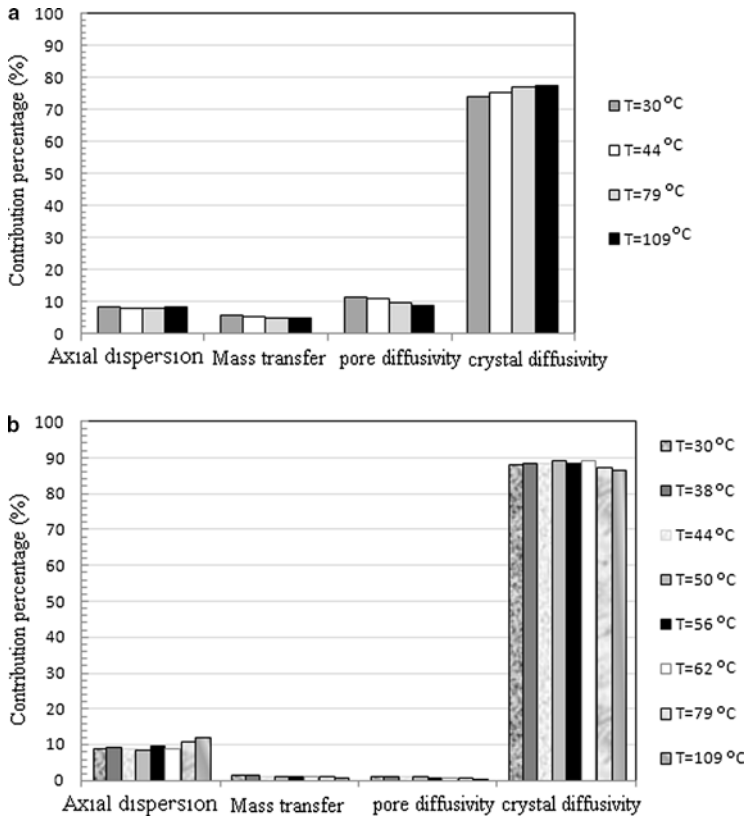

Fig. 11 Average contribution of each axial dispersion, mass transfer resistance and pore diffusivity upon the second central moments at various temperatures: (**a**) granulated nano-sized zeolite, (**b**) granulated micron sized zeolite

be concluded that the presence of the binder in granulated nano-zeolite resulted in strong resistance against diffusion of molecules into the zeolitic crystals and utilizing a suitable binderless granulation method was necessary to decrease the band broadening of response peak in a chromatography separation method.

With regards to the evaluated Henry's law constant (*i.e.*, provided in Table 2) as well as effective crystal diffusivity (*i.e.*, shown in Table 4) and parameters predicted by Eqs. (6)–(11); the second central moments were calculated according to its theoretical equation and results were plotted versus the experimental ones (Fig. 9). Although the error in the results of binderless granulated macron sized zeolite was higher than those of granulated nano-NaY, this comparison showed a good agreement between calculated and experimental second central moments.

The temperature dependency of crystal diffusivity was shown through Eq. (17). Therefore, for evaluation of the activation energy of effective crystal diffusivity (E_μ) and diffusivity constant ($D_{\mu 0}$), the logarithm of effective diffusivity values plotted versus the reciprocal absolute temperature as shown in Fig. 10. In this figure the minimum and maximum deviations from the mean value were also presented. Through the slope and intercept of this straight line, the activation energy of diffusion as well as; the diffusion constant were evaluated; respectively. Results were shown in Table 5.

$$D_\mu = D_{\mu 0} \exp\left(-\frac{E_\mu}{RT}\right) \tag{17}$$

The activation energies for crystal diffusivities were nearly similar for binderless and granules with 25 wt% of bentonite. This was also observed by another group of researchers (Breck 1974). Nevertheless, the somewhat of an enhancement in diffusion activation energy in the case of granulated nano-NaY in comparison with binderless gran-

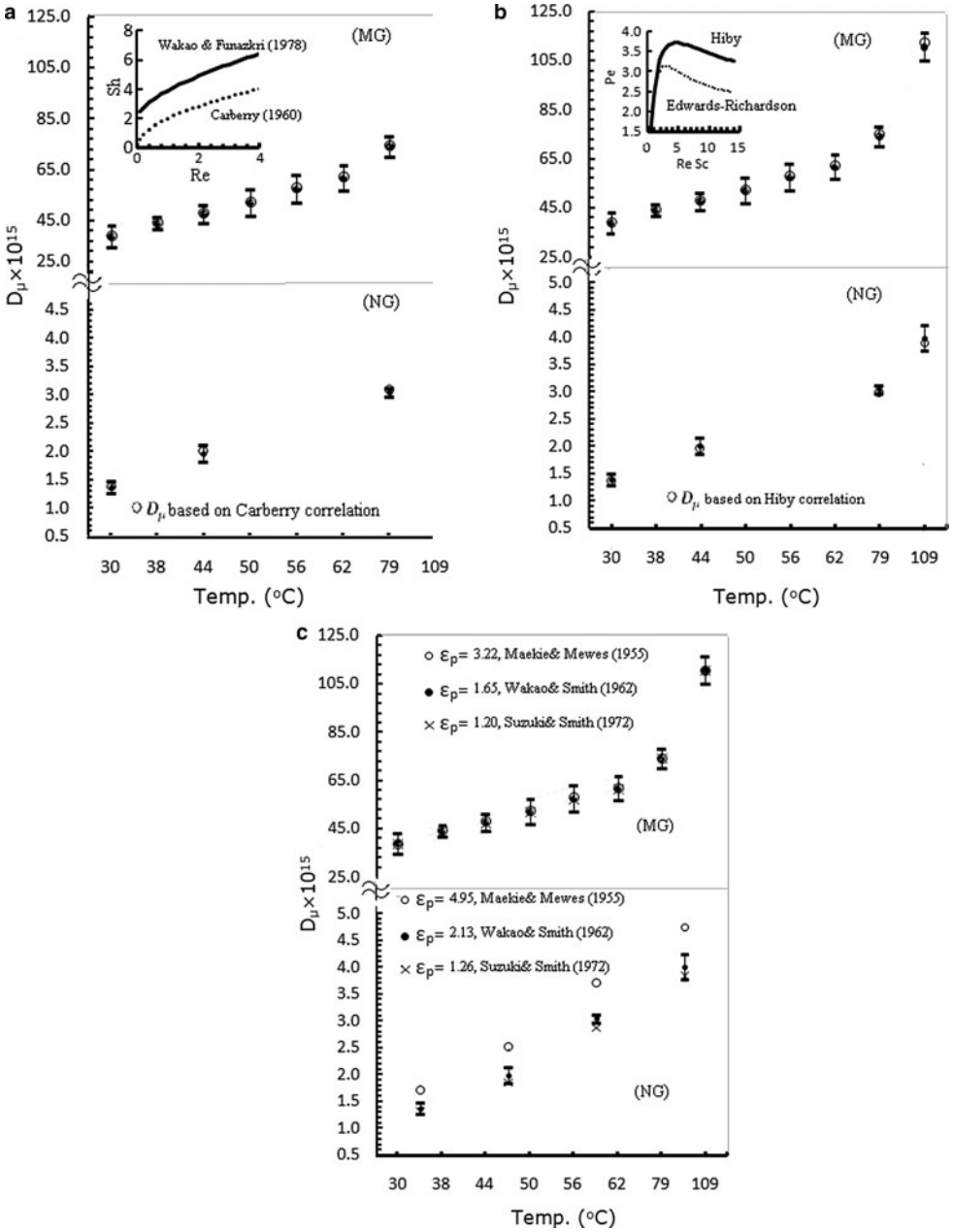

Fig. 12 The effect of various correlations on D_μ value, (**a**) effect of Sherwood number, (**b**) effect of Peclet number, (**c**) effect of tortuosity on D_μ. (The temperature axis is not scaled) (MG: granulated micronsized sized, NG: granulated nanosized zeolite)

ules of macron sized NaY may be attributed to the lower Si/Al molar ratio of zeolite in the former compared to latter.

In order to be confident in the obtained results, the contributions of various transfer resistances on the band broadening was calculated and demonstrated in Fig. 11. Results indicated that at velocities selected in the range of 9 to 31 cm/s, such effects for each of the axial dispersion, mass transfer resistance and pore diffusion upon the band broadening was less than 10 % of the second central moment. Hence, discrepancies in selected correlations are not likely to cause significant errors. Moreover, the effect of various well known correlations of extracrystalline resistances on values of D_μ was investigated. As shown in Fig. 12, decrease in mass transfer coefficient up to 68 % and increase in axial dispersion coefficients up 30 % demonstrated no significant errors on calculated values of the D_μ. Nonetheless; increasing tortuosity factor from 2.11 to 4.95 resulted in higher error on the values of D_μ in the case of the granulated nano-sized zeolite. It is noteworthy that, due to the difference in granules dimensions, the effect of tortuosity correlation on D_μ in granulated micron sized zeolite was less than granulated nano-sized one. Nevertheless, it was observed that in the case of granulated nano-zeolite the standard error of D_μ as well as; the activation energy of diffusion at various temperatures increased by enhancing the tortuosity factor such that the trend in the temperature de-

pendency of D_μ became unreasonably reversed at tortuosity factor higher than 9. Accordingly, at lower extents of tortuosity factor, better agreement between experimental results and predicted values was obtained. Consequently, the accuracy of obtained results at lower values of this factor was confirmed.

The difference observed between the D_μ values of present and previously published results (*i.e.*; PFG NMR technique Heink et al. 1990) attributed to the utilized method. For many systems the apparent intra-crystalline diffusivity depends upon the length scale over which the diffusivity is measured (Cejka et al. 2007). Furthermore, the smaller obtained values of D_μ may be due to the underestimated extracrystalline resistances or existence of an additional resistance on the outer surface of zeolitic crystals. As discussed previously no change observed in the order of magnitude of D_μ values by utilizing various well known correlations of extracrystalline resistances. Therefore, underestimated extracrystalline resistances might not have been the reason for this discrepancy. On the other hand, the other possibility which states that sorption rate may be controlled by both surface resistance and intracrystalline diffusion is inconsistent with the results obtained by Pfeifer et al. (1990). Although they observed a transport resistance on the external surfaces in diffusion of Xe into the ZSM-5 and NaCaA crystals, no surface resistance was observed in their case of NaX zeolite. Nevertheless, surface barriers might have occurred after hydrothermal treatment performed during granulation process in the present work. Moreover, in the case of granulated nano-zeolite the presence of the binder surrounded the zeolite crystals might have added an additional resistance to mass transfer of the Xe species. These might be the reason for the aforementioned discrepancy. Furthermore, it is noteworthy that the results obtained by methods such as QENS and PFG NMR which directly probe the microscopic mechanism of diffusion provide the most interesting information from a fundamental point of view. These methods, however, are of little use when obtained results may not be directly related to the properties of such systems on a laboratory or even an industrial scale. Consequently, values determined in this research in comparison with D_μ obtained by microscopic methods were more reliable and applicable for simulation of real chromatography columns usually filled with composite granules of zeolite and inorganic binder of bentonite. Furthermore, it should be noted that a given simulation results utilizing this study's estimated Henry's law constant and crystal diffusivity may have the highest precision when other diffusion parameters including; D_{ax}, K_m, D_p and D_{AB} could be predicted by the empirical expressions applied in this work. In other words, a complete set of adsorption and diffusion parameters needed to simulate the chromatography columns was presented in this work with the precision shown in Fig. 9.

5 Conclusion

In this study the Henry's law constant and crystal diffusivity of xenon in the granulated nano-NaY with 25 % binder were precisely measured and compared with values obtained for binderless granules of micron sized NaY. Results of this comparison revealed that the binder behaved as an inert diluent with no significant effect on the adsorption capacity of nano crystals while it led to enhancing the intra-crystalline diffusion resistance. The effective crystal diffusivity in granules with 25 wt% of the binder was determined to be 96 percent lower than the binderless granules. The activation energies of crystal diffusivity of xenon in the granulated nano-NaY zeolite and binderless granules of micron sized NaY zeolite were also evaluated to be 12.76 ± 0.91 and 12.63 ± 1.11 kJ/mol; respectively. In addition, the heat of adsorption of xenon in these adsorbents was determined to be 17.61 ± 0.38 and 17.43 ± 0.38 kJ/mol; respectively. It is reiterated that, all these values will be needed when separation optimization is sought theoretically. This latest issue is currently under investigation in these authors laboratory.

References

Armatas, G.S., Petrakis, D.E., Pomonis, P.J.: Estimation of diffusion parameters in functionalized silicas with modulated porosity. Part I. Chromatographic studies. J. Chromatogr. A **1074**, 53–59 (2005)

Breck, D.W.: Zeolite Molecular Sieves. Wiley, New York (1974)

Charkhi, A., Kazemeini, M., Ahmadi, S.J., Kazemian, H.: Granulation of nano-zeolites utilizing sodium alginate as an external template. In: 2nd International Iranin Zeolite Congress, Tehran, Iran (2010)

Cejka, J., Bekkum, H.V., Corma, A., Schuth, F.: Introduction to Zeolite Science and Particle. Studies in Surface Science and Catalysis vol. 168. Elsevier, Amsterdam (2007)

Delmas, M.P.F., Ruthven, D.M.: Measurement of intracrystalline diffusion in NaX zeolite by capillary column gas chromatography. Microporous Mater. **3**, 581–592 (1995)

Denayer, J.F.M., Baro, G.V.: Adsorption of normal and branched paraffins in faujasite zeolites NaY, HY, Pt/NaY and USY. Adsorption **3**, 251–265 (1997)

Dıaz, E., Ordonez, S., Auroux, A.: Comparative study on the gas-phase adsorption of hexane over zeolites by calorimetry and inverse gas chromatography. J. Chromatogr. A **1095**, 131–137 (2005)

Dıaz, E., Ordonez, S., Vega, A., Coca, J.: Adsorption characterisation of different volatile organic compounds over alumina, zeolites and activated carbon using inverse gas chromatography. J. Chromatogr. A **1049**, 139–146 (2004)

Do, D.D.: Adsorption Analysis: Equilibria and Kinetics. Imperical College Press, London (1998)

Giddings, J.C., Keller, R.A.: Dynamics of Chromatography. Part I. Principle and Theory. Dekker, New York (1965)

Guiochon, G., Felinger, A., Shirazi, D.G., Katti, A.M.: Fundamentals of Preparative and Nonlinear Chromatography, 2nd edn. Elsevier, Netherlands (2006)

Heink, W., Kaerger, J., Pfeifer, H., Stallmach, F.: Measurement of the intracrystalline self-diffusion of xenon in zeolites by the NMR pulsed field gradient technique. J. Am. Chem. Soc. **112**, 2175–2178 (1990)

Inel, O., Topaloglu, D., Askın, A., Tümsek, F.: Evaluation of the thermodynamic parameters for the adsorption of some hydrocarbons on 4A and 13X zeolites by inverse gas chromatography. Chem. Eng. J. **88**, 255–262 (2002)

Kang, Y., Shan, W., Wu, J., Zhang, Y., Wang, X., Yang, W., Tang, Y.: Uniform nano-zeolite microspheres with large secondary pore architecture. Chem. Mater. **18**, 1861–1866 (2006)

Karger, J., Ruthven, D.M.: Diffusion in Zeolites and Other Microporous Solids. Wiley, New York (1992)

Mosell, T., Schrimpf, G., Brickmann, J.: Xenon diffusion in zeolite NaY:transition-state theory with dynamical corrections. J. Phys. Chem. **100**, 4582–4590 (1996)

Perry, R.H., Green, D.W.: Perry's Chemical Engineer's Handbook. McGraw-Hill, New York (1999)

Pfeifer, H., Freude, D., Kaerger, J.: Catalysis and Adsorption by Zeolites. Studies in Surface Science and Catalysis vol. 65. Elsevier, Amsterdam (1990)

Schmidt-Traub, H.: Preparative Chromatography of Fine Chemicals and Pharmaceutical Agents. Wiley-VCH, Mühlenbach (2005)

Tosheva, L., Valtchev, V., Sterte, J.: Silicalite-1 containing microspheres prepared using shape-directing macro-templates. Microporous Mesoporous Mater. **35–36**, 621–629 (2000)

Valtchev, V., Mintova, S.: Layer-by-layer preparation of zeolite coating of nanosized crystals. Microporous Mesoporous Mater. **43**, 41–49 (2001)

Zhang, J., Zhao, Z., Duan, A., Jiang, G., Liu, J., Zhang, D.: Chromatographic study on the adsorption and diffusion of light hydrocarbons in ZSM-5 and USY zeolites. Energy Fuels **23**, 617–623 (2009)